

## CHAPTER 4

### Results and discussions

#### 4.1 Characterization of vertically aligned ZnO nanowires

As shown in chapter 3, two interesting parameters in preparation of vertically aligned ZnO nanowires were considered consisting of growth temperature and acetone flow rate. Then, the synthesis products were characterized by field emission scanning electron microscopy (FE-SEM) and x-ray diffractometry (XRD). Finally, the vertically aligned ZnO nanowires were fabricated as an ethanol sensor.

##### 4.1.1 Characterization of morphology by scanning electron microscopy

###### Group 1: varied growth temperature

Investigating on the average diameter of ZnO nanowires was carried out by FE-SEM. A carbon tape will be stucked on the border of the samples in order to improve resolution and prevent charging. FE-SEM images of the ZnO nanowires synthesized in different growth temperatures of 400°C – 550°C under fixed acetone atmosphere in 5 sccm of flow rate are shown in Figure 4.1- 4.4.

ลิขสิทธิ์มหาวิทยาลัยเชียงใหม่  
Copyright© by Chiang Mai University  
All rights reserved

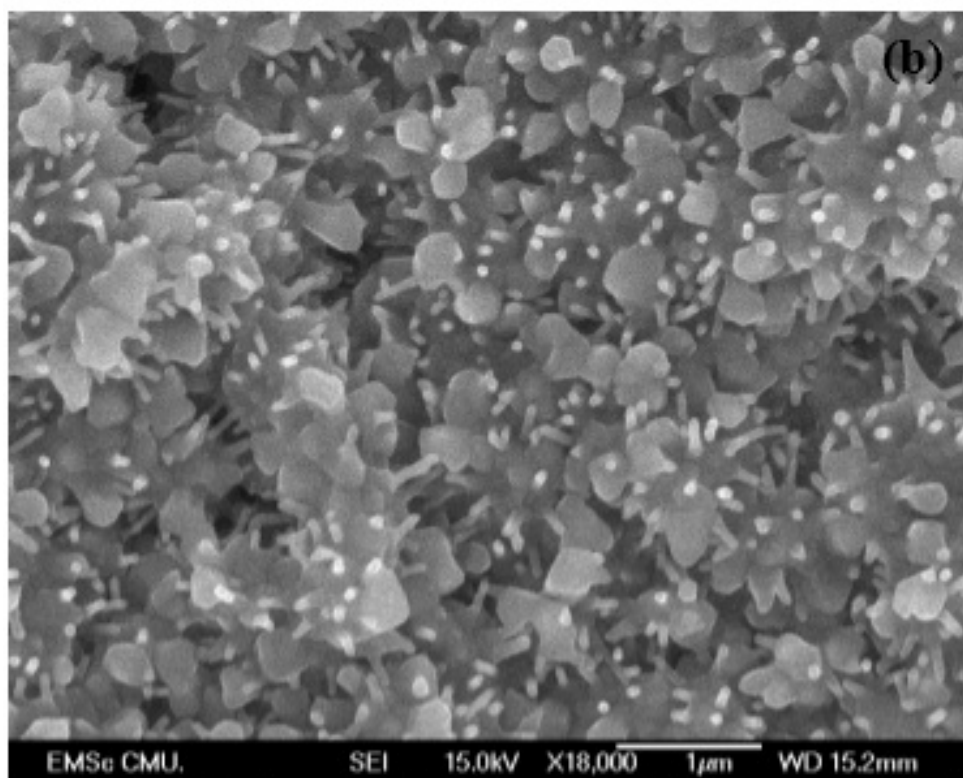
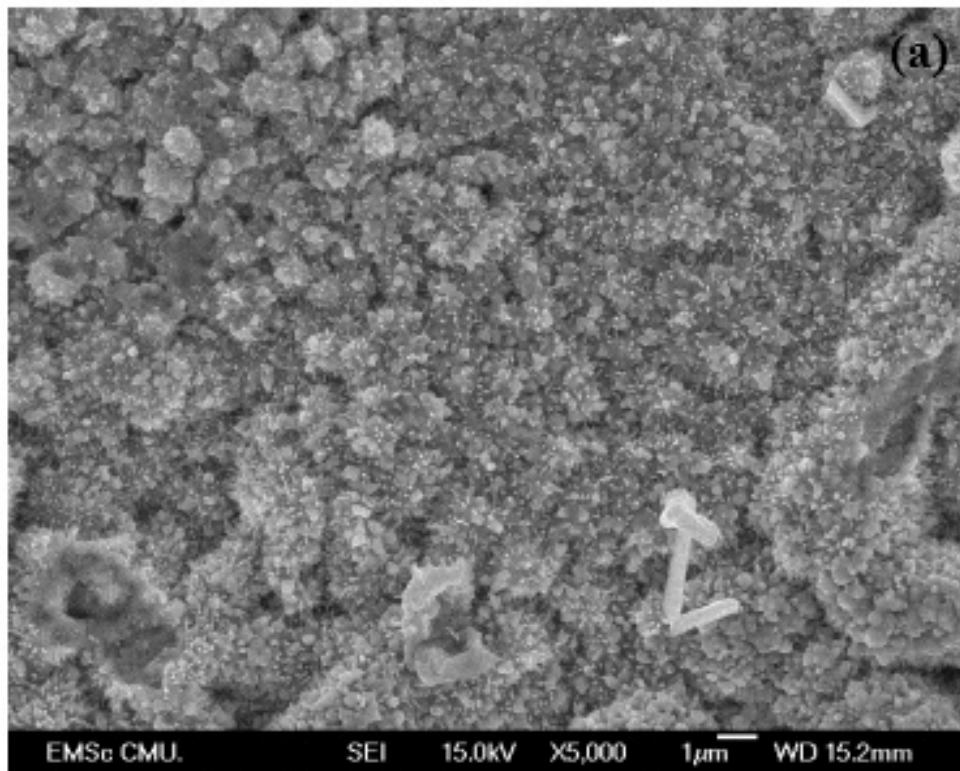


Figure 4.1: FE-SEM images at 400°C growth temperature at different magnitudes (a) x5,000 and (b) 18,000

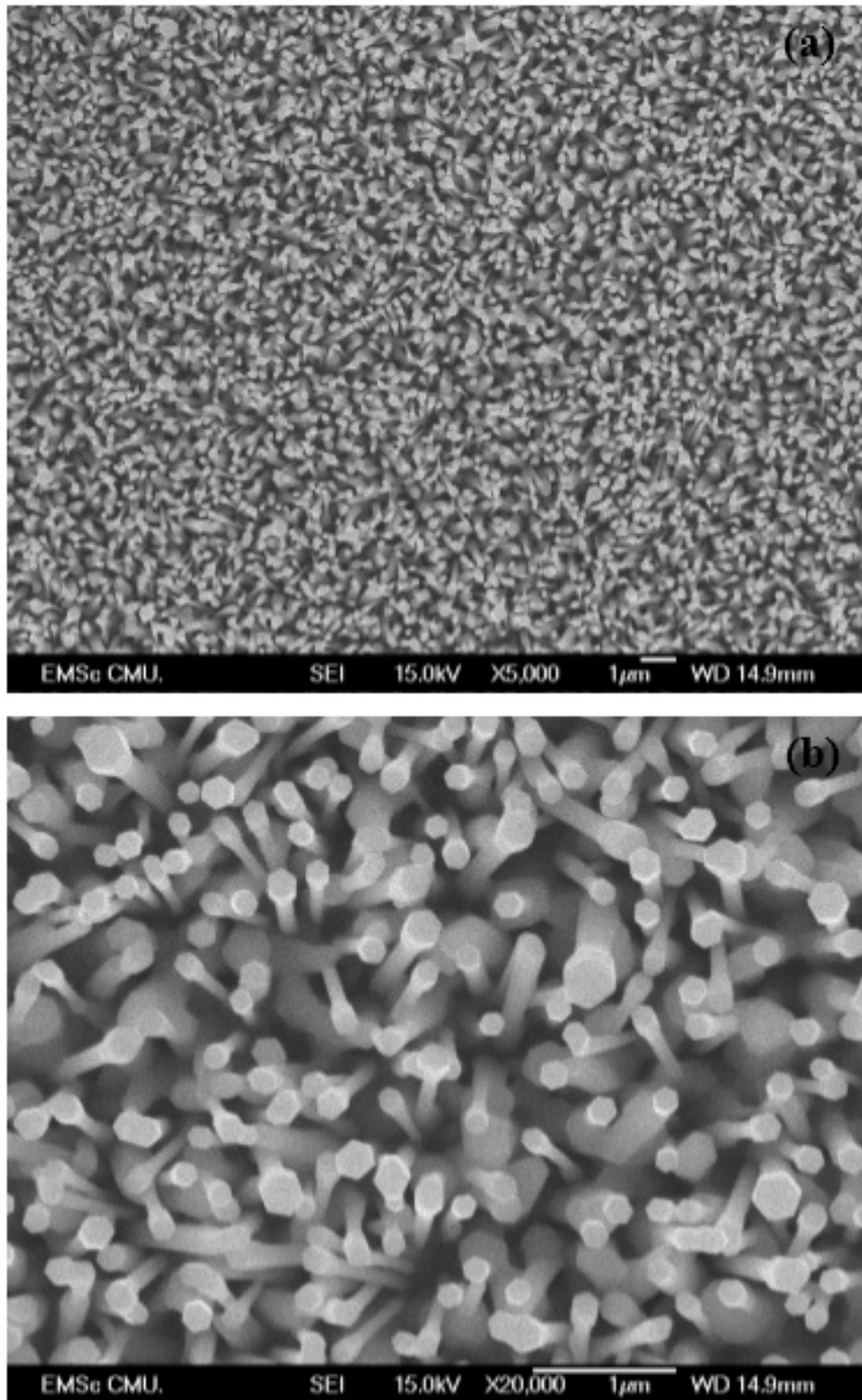


Figure 4.2: FE-SEM images at 450°C growth temperature at different magnitudes (a) x5,000 and (b) 20,000

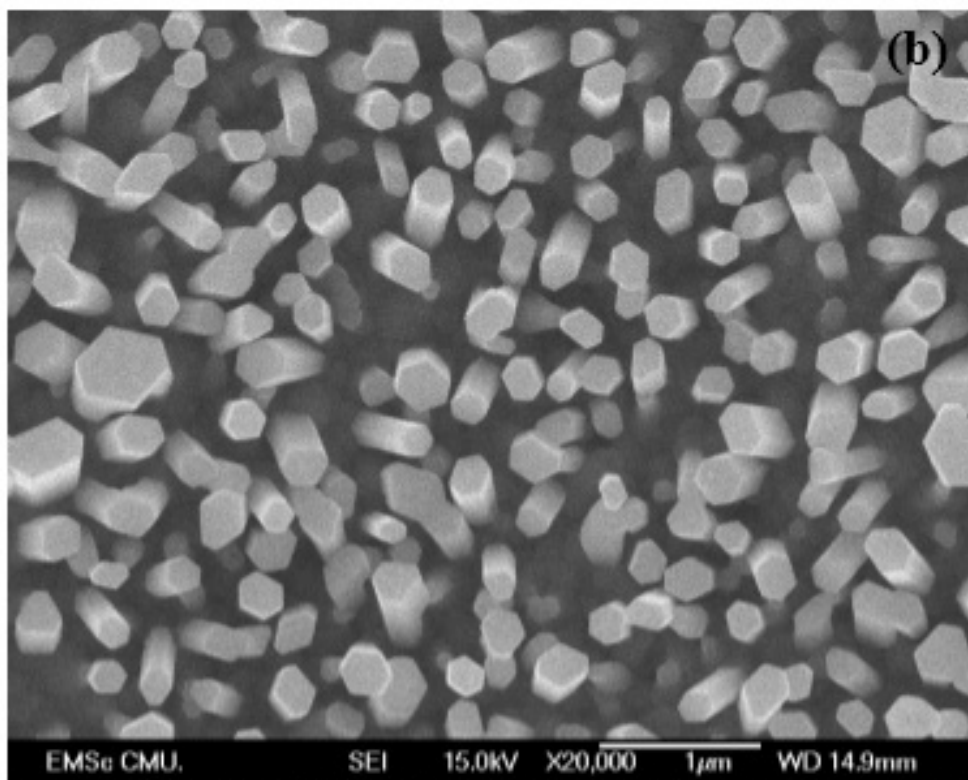
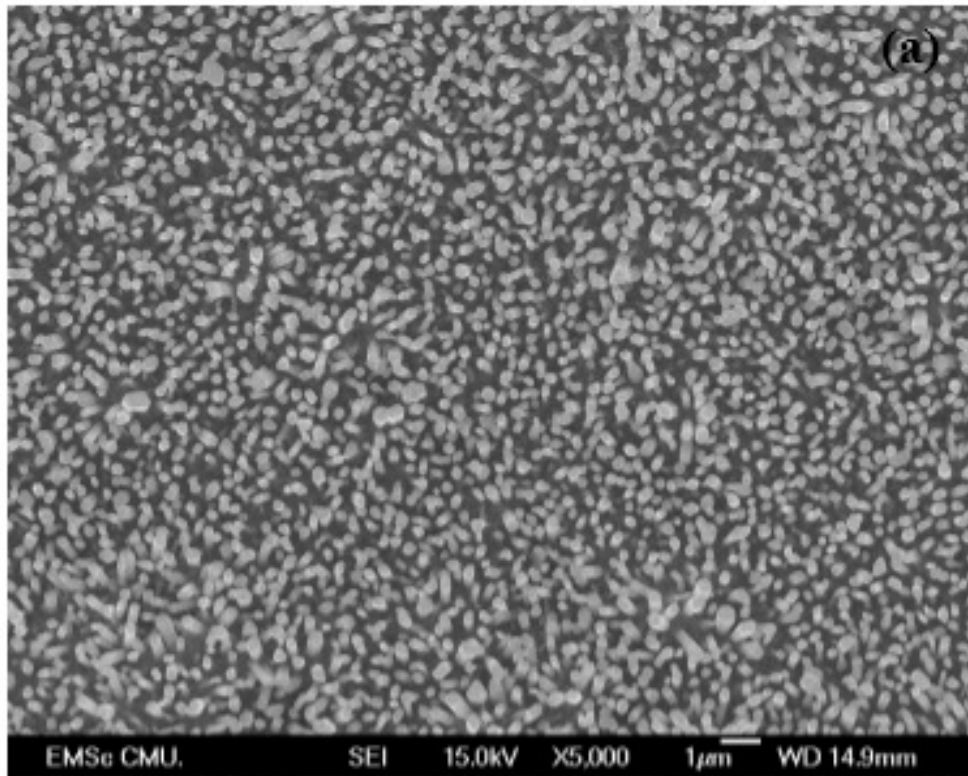


Figure 4.3: FE-SEM images at 500°C growth temperature at different magnitudes (a) x5,000 and (b) 20,000

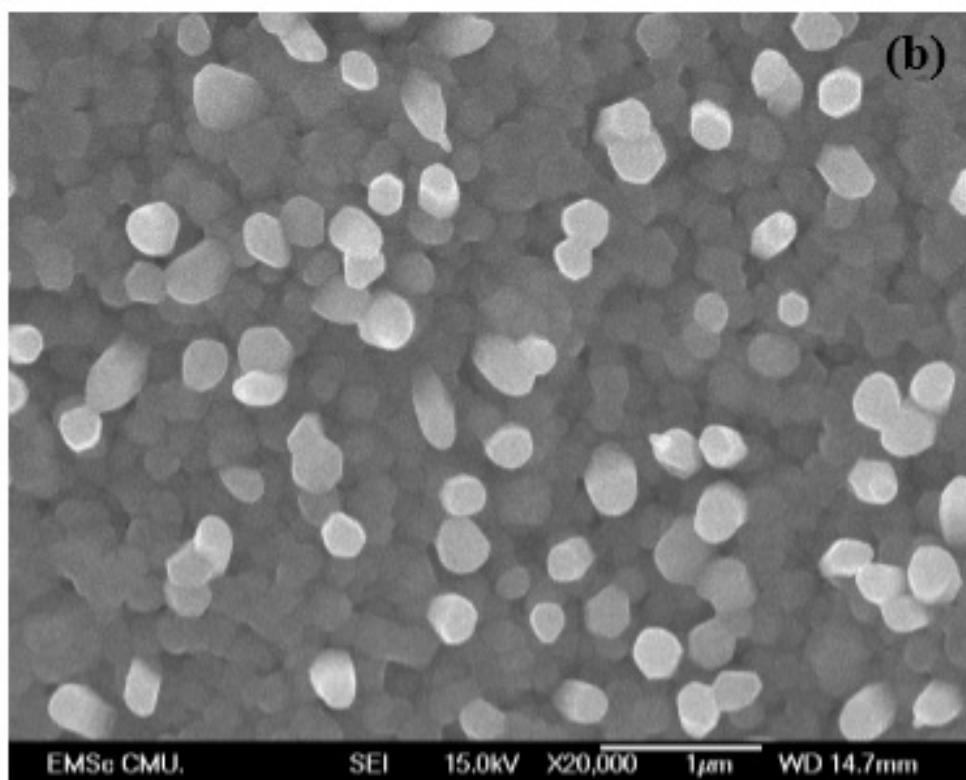
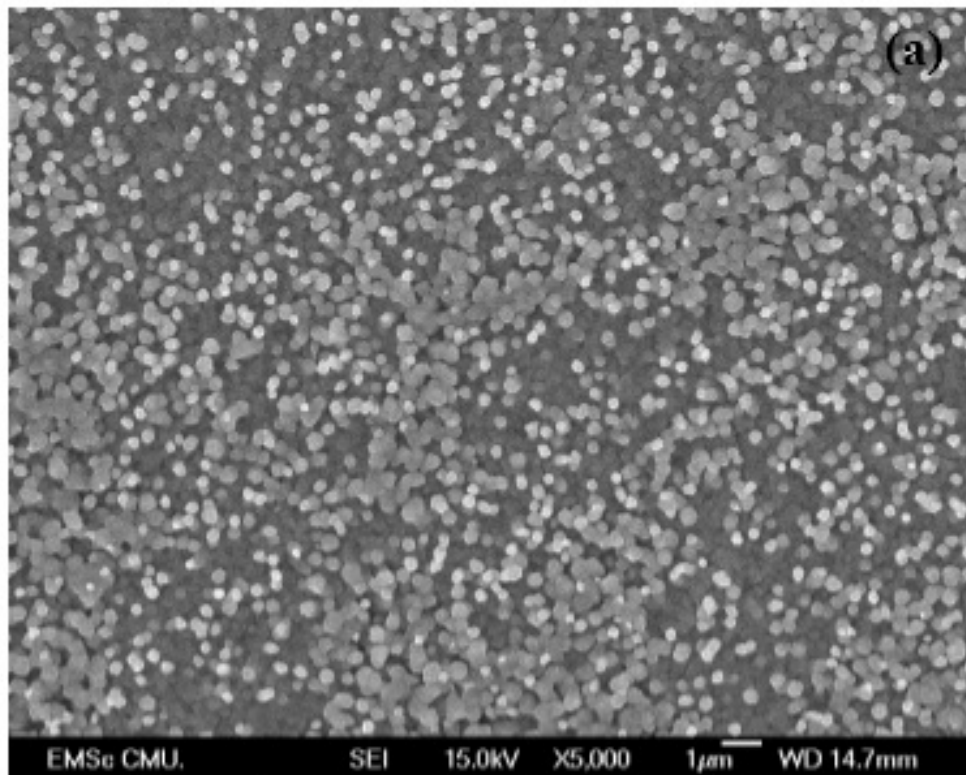


Figure 4.4: FE-SEM images at 550°C growth temperature at different magnitudes (a) x5,000 and (b) 20,000

Figure 4.1 - 4.4 demonstrated that the density of ZnO nanowires increases while temperature raises up. Furthermore, the uniformity of ZnO nanowires in each growth temperature also increases. This result is in good agreement with the work by S. Choopun et.al.<sup>(1)</sup> in which the density of ZnO nanowires is represented by nuclei probability given by Eq. (2.14). It can be seen that the probability increases when temperature increases. Therefore, growth temperature affects to oxidization in forming ZnO-nanowires. The results also show that the nanowires are uniformity and well aligned on the glass substrate at growth temperature 550°C, 500°C, and 450°C. While at growth temperature 400°C, FE-SEM reveals the low density of ZnO nanowires due to growth temperature below melting point of Zn. Thereby, the Zn was ionized lower than other temperature conditions as shown Figure 4.5.

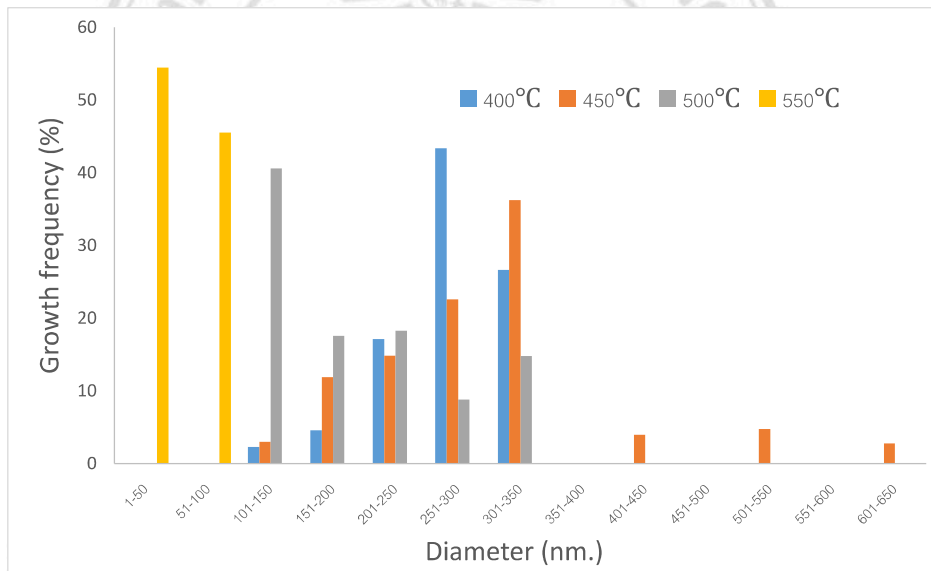


Figure 4.5: Growth frequency of ZnO nanowires at various temperatures

The ZnO nanowires as shown in Figure 4.1, grown in growth temperature of 400°C, have an average diameter of  $56.30 \pm 1.99$  nm. The second condition of nanowires synthesized at growth temperature of 450°C, has an average size of  $173.60 \pm 5.93$  nm (Figure 4.2), while the average diameter of the third and fourth condition of nanowires at growth temperature of 500°C and 550°C, was observed to be  $261.39 \pm 8.76$  nm (Figure 4.3) and  $254.11 \pm 4.901$  nm (Figure 4.4), respectively. The average diameter and the size distribution of each conditions of ZnO nanowires were calculated based on nanowires counted.

The FE-SEM images show that the diameter of ZnO nanowires increases while rising up growth temperature. Because of growth temperature effect, nuclei probability governs to increase and ZnO nuclei will be occurred plentifully. Moreover, ZnO nuclei will fuse and connect nearby nuclei, consequently forming larger nuclei. The average diameters are shown in Table 4.1

Table 4.1: Average diameter of the vertically aligned ZnO nanowires

Temperature ( $^{\circ}C$ )	Average diameter (nm.)	Standard error
400	56.30	1.987
450	173.60	5.93
500	261.39	8.761
550	254.11	4.901

Group 2: varied acetone flow rate

FE-SEM images of the ZnO nanowires on glass substrate with zinc acetate dehydrate seeding layer, grown at deposition temperature  $500^{\circ}C$  under various acetone atmosphere by flow rate in range of 5 sccm to 45 sccm, are shown in Figure 4.6- 4.8.

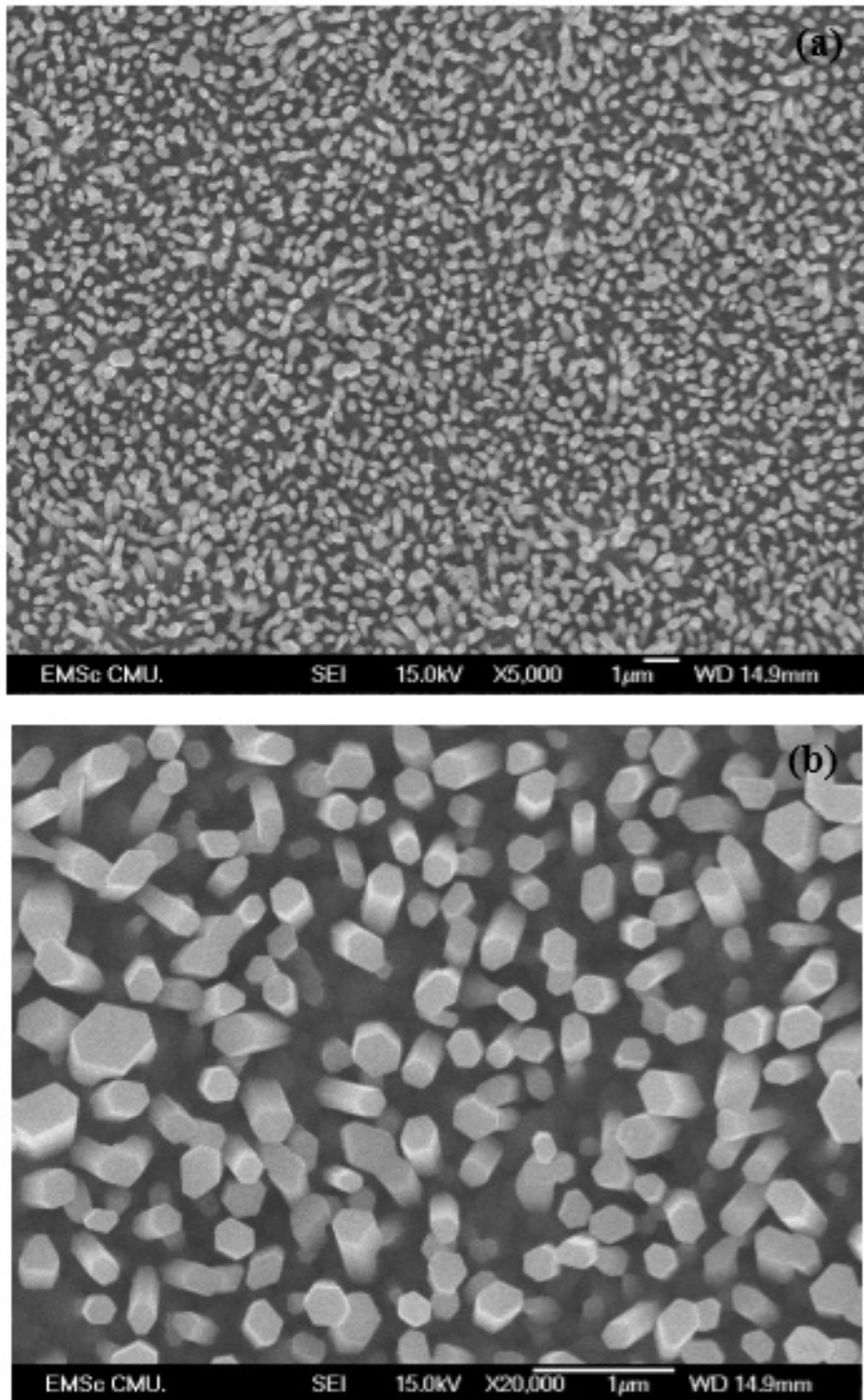


Figure 4.6: FE-SEM images with 5 sccm acetone flow rate at different magnitudes (a) 5,000 and (b) 20,000



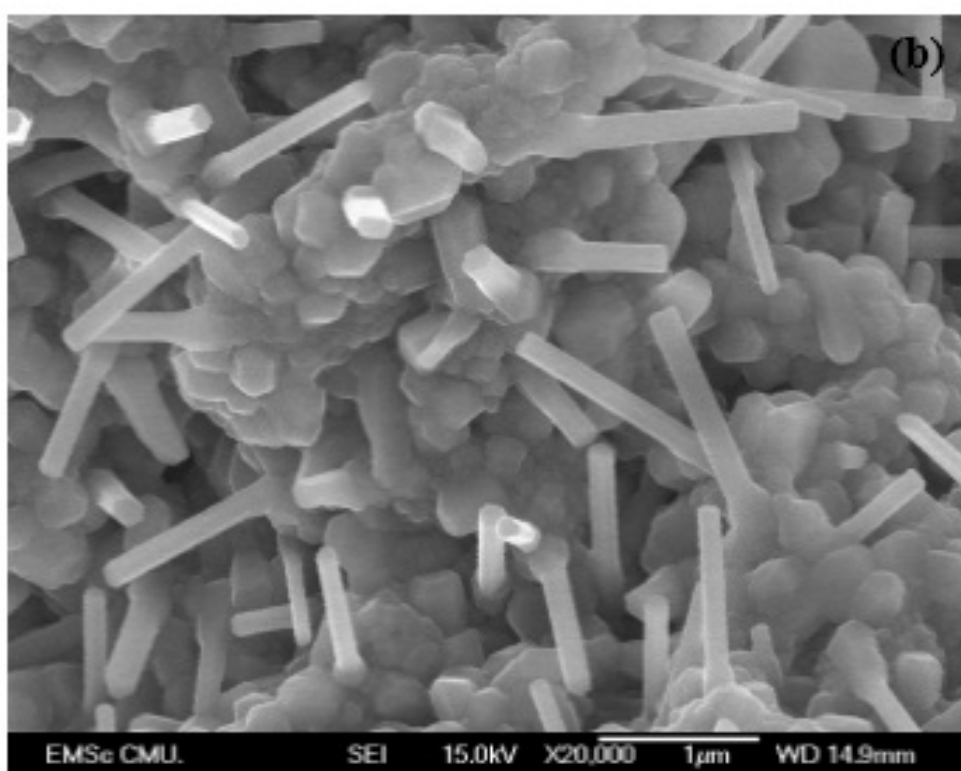
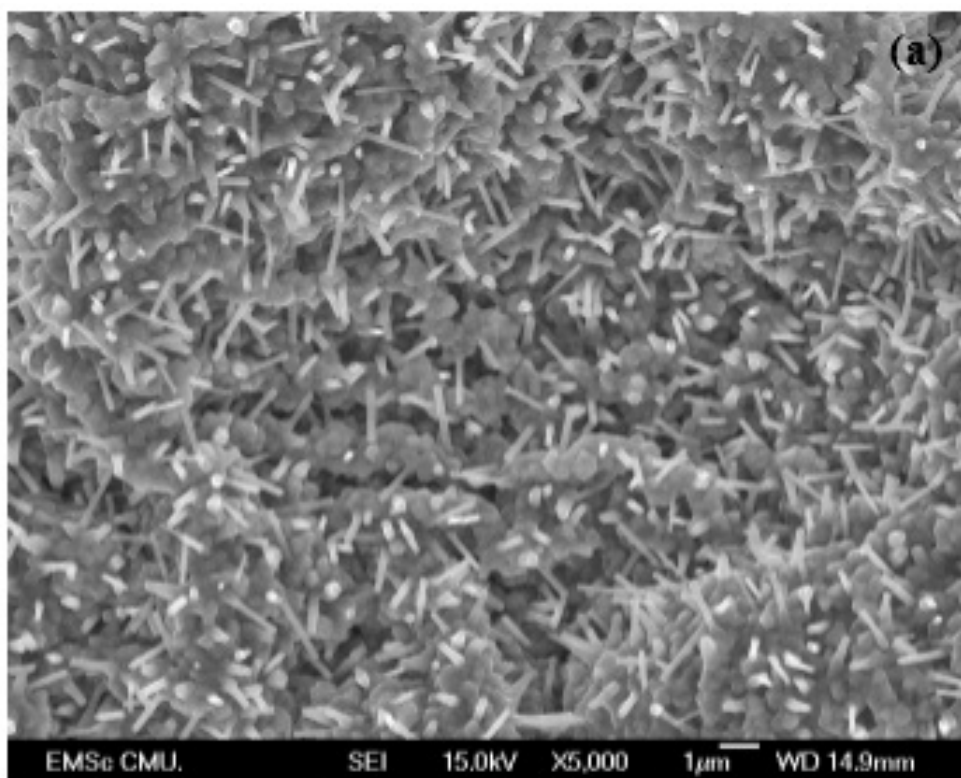


Figure 4.7: FE-SEM images with 15 sccm acetone flow rate at different magnitudes (a) 5,000 and (b) 20,000

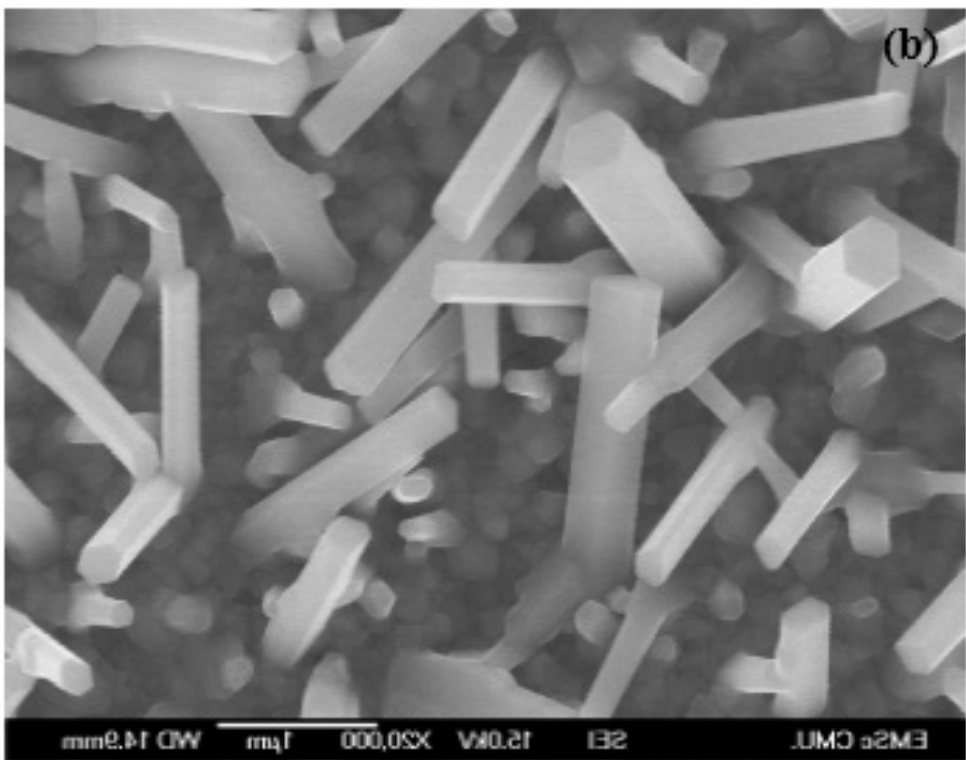
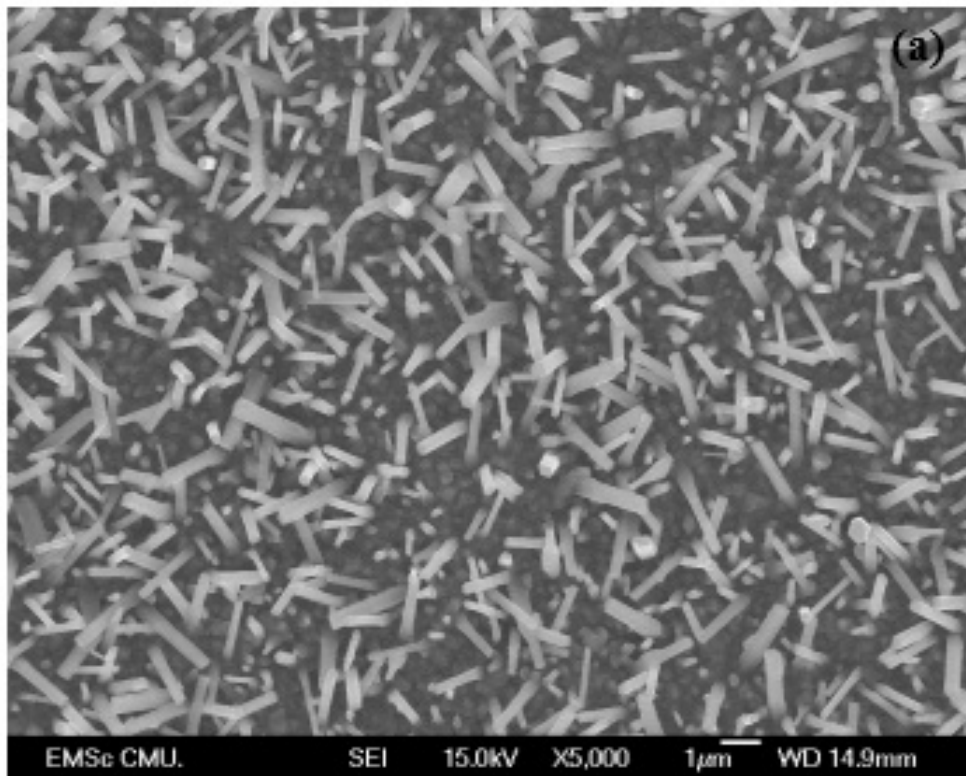


Figure 4.8: FE-SEM images with 45 sccm acetone flow rate at different magnitudes (a) 5,000 and (b) 20,000

Figure 4.6 – 4.8 demonstrated that the diameter of ZnO nanowires decreases while acetone flow rate increases. In addition, the uniformity of ZnO nanowires and feasibility of vertical aligned ZnO nanowires also decreases. Acetone flow rate which was interesting parameter in group 2, represents the partial pressure of the oxygen which is the source of oxidation reaction. From the result, it was found that raising up the acetone flow rate in the synthesized process influences to decreasing the diameter of ZnO nanowires. The variety of diameter of ZnO nanowires in each condition of acetone flow rate is shown in Figure 4.9 and Average of diameter in condition of acetone flow rate was shown in Table 4.2.

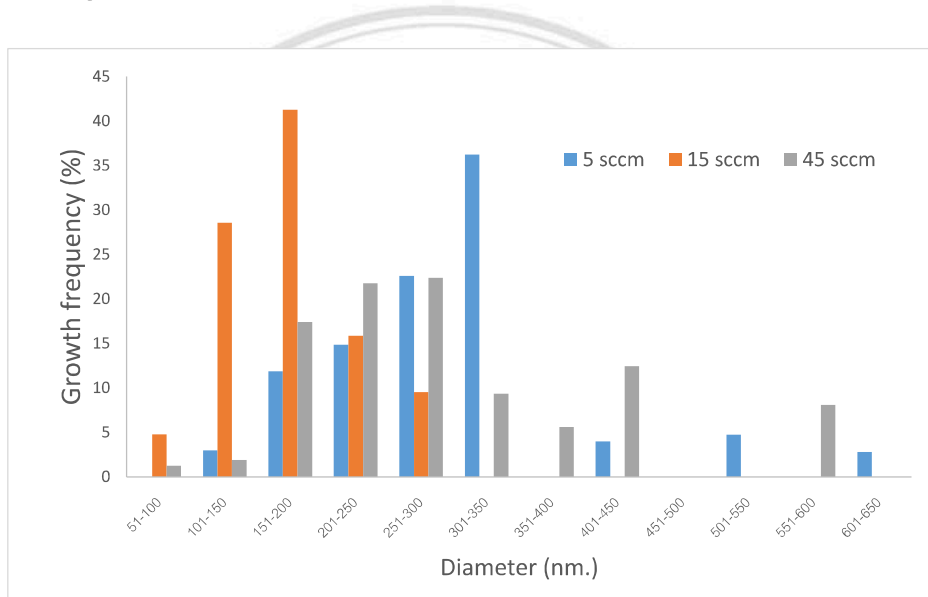


Figure 4.9: Growth frequency of ZnO nanowires at various acetone flow rates

Table 4.2: Average diameter in different conditions of acetone flow rate

Acetone flow rate (sccm.)	Average diameter (nm.)	Standard error
5	261.39	8.76
15	190.88	5.31
45	208.70	9.73

The ZnO nanowires shown in Figure 4.6, grown in acetone flow rate of 5 sccm, has an average diameter of  $261.39 \pm 8.76$  nm. The second condition of nanowires synthesized in acetone flow rate of 15 sccm, has an average size of  $190.88 \pm 5.31$  nm (Figure 4.7), while the average diameter of the third condition of nanowires grown in acetone flow rate of 45 sccm, was observed to be  $208.70 \pm 9.73$  nm (Figure 4.8). The increasing of acetone

flow rate implies an increase in supersaturation level reaching to decrease the Gibb free energy change per volume and the size of the critical radius. Eventually, the total Gibb free energy change per nuclei becomes to low value and fast nucleation formation.

#### 4.1.2 Characterization of crystallinity by x-ray diffractometry

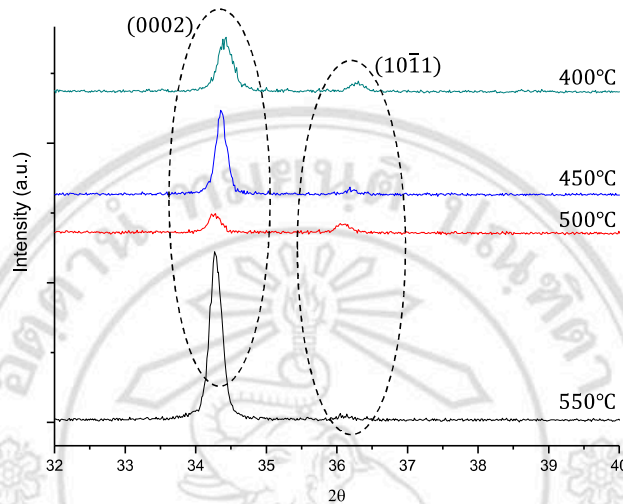


Figure 4.10: XRD result of ZnO nanowires at various growth temperatures

The crystallographic structure of the synthetic ZnO nanowires was characterized by XRD with  $2\theta$  range of 32-40 degree. Figure 4.10 shows the XRD pattern of the ZnO nanowires synthesized on glass slide substrate that consists of various growth temperature. The XRD pattern shows that all the peaks can be indexed to hexagonal wurtzite ZnO (JCPDS card No. 89-13971) with lattice parameter  $a = 3.48 \text{ \AA}$  and  $c = 5.20 \text{ \AA}$ . It demonstrated a strongly preferential orientation in the  $c$  axis, indicating (0002) and (10-11) directions and suggests good crystallinity. Moreover, the high intensity on  $c$  axis was suggested growing to be vertically aligned nanowires.

#### 4.2 Fabrication and investigation of vertically aligned ZnO nanowires gas sensors using ethanol vapor

The condition of 500°C growth deposition under acetone flow rate of 5 sccm are selected from main experiment to test sensitivity with ethanol vapor. The sensor devices

based on vertically aligned ZnO nanowires were manufactured by putting gold paste as electrodes on the top of surface above ZnO nanowires. Two electrodes were put on the top and the end of sample before annealing under temperature of 50°C. The resistance response and recovery of sensor showed to ethanol concentration of 500 ppm at operating temperature of 350°C to 550°C. The resistance of sensor decreased dramatically when releasing ethanol vapor and recovered to the initial resistance after removing ethanol vapor. All sensor exhibited the difference of changing resistance pattern. The sensor response at 500 ppm of ethanol concentration are plotted as a function of resistance and time as shown in Appendix A.

As a result, it can be seen that the tendency of the average sensitivity grew up while increasing the operating temperature. In the same time, the average response time and average recovery time decreased. Figure 4.11 demonstrated the average sensitivity in each condition. It can be seen that the sensor exhibited the highest sensor response at 500°C.

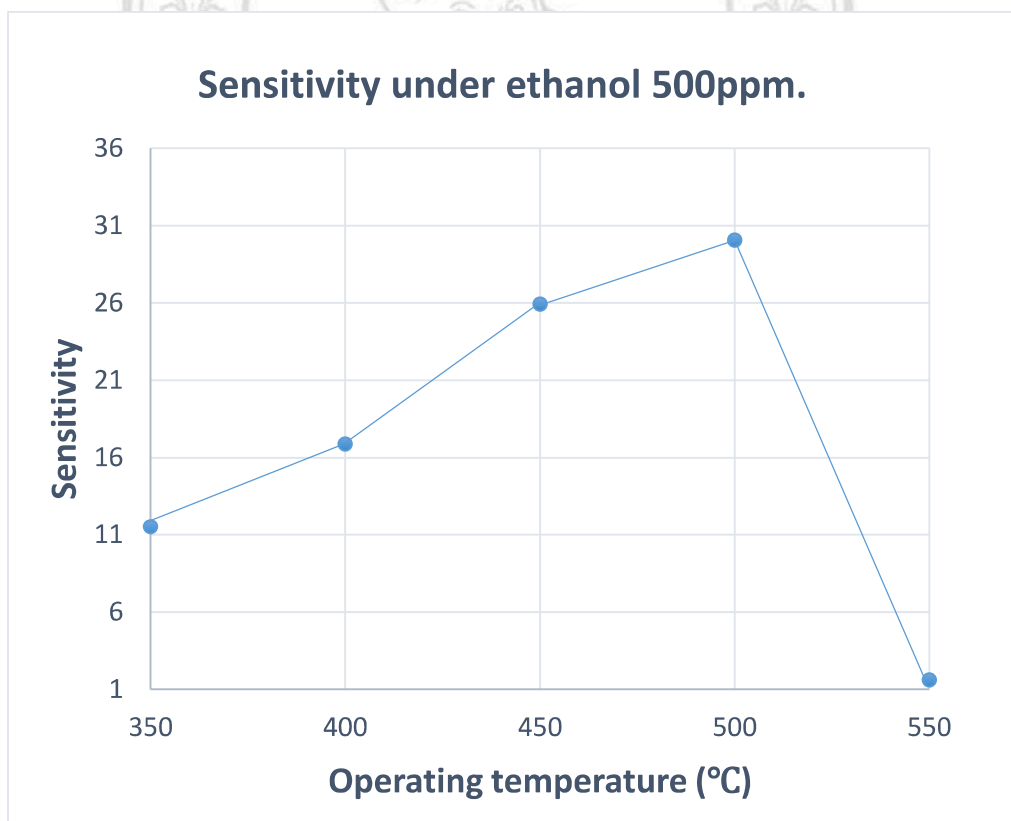


Figure 4.11: Average sensitivity at various operating temperature

Some samples in condition of operating of 500°C and 550°C were melted. Because of using in high operating temperature for long time, the electrode contact peeled off or got failure at contact. In order to simplify consideration, these sample were not approved as shown as Table 4.3. Totally, sensor response increased while temperature increased and optimum temperature was at 500°C and as all results can be implied that the limitation of sensor was located by melting of substrate close to 550°C.

Table 4.3: Sensitivity at various operating temperatures

Operating Temperature (°C)	Sample 1	Sample 2	Sample 3	Average sensitivity	Standard error
350	9.34	12.79	12.42	11.52	1.09
400	18.81	16.86	16.96	16.88	0.05
450	25.50	25.90	26.40	25.93	0.26
500	28.84	31.31	-	30.08	1.23
550	1.60	-	-	1.60	-

Response time and recovery time are another factor used to estimate the performance of gas sensors device, defined as the time taken to achieve 90% of the final change in resistance following the change of gas concentration. Table 4.4 shows the response time and recovery time of the ZnO nanowires to 500 ppm of ethanol vapor at various operating temperatures

Table 4.4: Response and recovery time at various operating temperatures

Operating temperature (°C)	Response time( s. )	Recovery time ( s. )
350	5.50	970.03
400	3.62	229.52
450	1.80	67.62
500	1.98	49.00

From the table, it can be seen that the response time of the gas sensors decreases as the increasing temperature, as expected from the reaction rate constant as shown in Eq. (2.15) At operating temperature of 350°C, the sensors need 5.5 seconds to response with 500 ppm ethanol vapor. While at higher temperatures, it takes lower response time. Moreover, the recovery time shows similar tendency while increasing operating temperature and reveal the high sensitivity and short response and recovery time.